Electronic Supplementary Material (ESI) for Nanoscale.

Supplementary Information for:

Hybrid vanadate waveguiding configurations for extreme optical confinement and efficient polarization management in the near-infrared

Yusheng Bian[1,2], Lei Kang[1], Qiang Ren[3], Yuanxia Zheng[5,6], Roman Engel-Herbert[4,5,7], Pingjuan L. Werner[1], Douglas H. Werner[1,5]*, Ajey P. Jacob[2] and Abu Thomas[2]

[1]Computational Electromagnetics and Antennas Research Lab (CEARL)

Department of Electrical Engineering, The Pennsylvania State University

University Park, PA, 16802, USA

[2]Globalfoundries, 400 Stone Break Rd. Extension, Malta, NY 12020, USA

[3]School of Electronics and Information Engineering, Beihang University

Beijing 100191, China

[4]Department of Materials Science and Engineering

The Pennsylvania State University, University Park, PA 16802, USA

[5]Materials Research Institute, The Pennsylvania State University

University Park, PA 16802, USA

[6]Department of Physics, The Pennsylvania State University

University Park, PA 16802, USA

[7]Department of Chemistry, The Pennsylvania State University

University Park, PA 16802, USA

**Corresponding Author. Email:dhw@psu.edu*

S1. Permittivities of $CaVO_3$ and $SrVO_3$

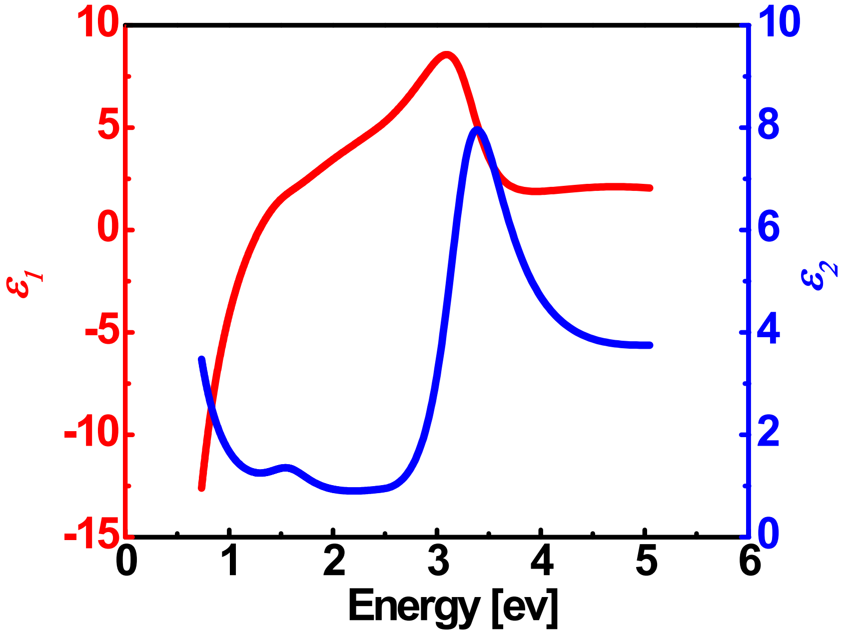

Supplementary Figure 1. Real part (ε_1) and imaginary part (ε_2) of the relative permittivity of $CaVO_3$.

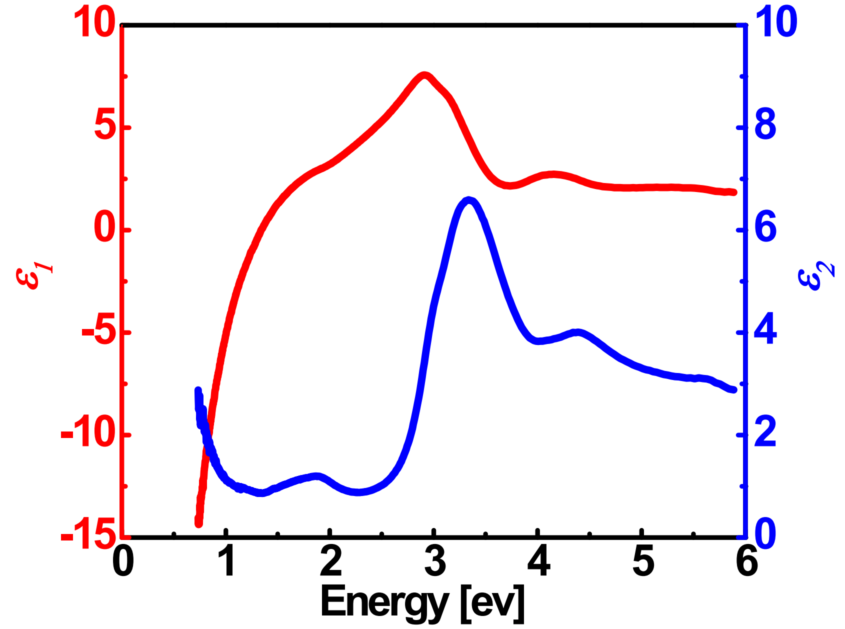

Supplementary Figure 2. Real part (ε_1) and imaginary part (ε_2) of the relative permittivity of $SrVO_3$.

S2. Mode dispersion at CaVO$_3$/dielectric interfaces and comparison with other two-layer systems

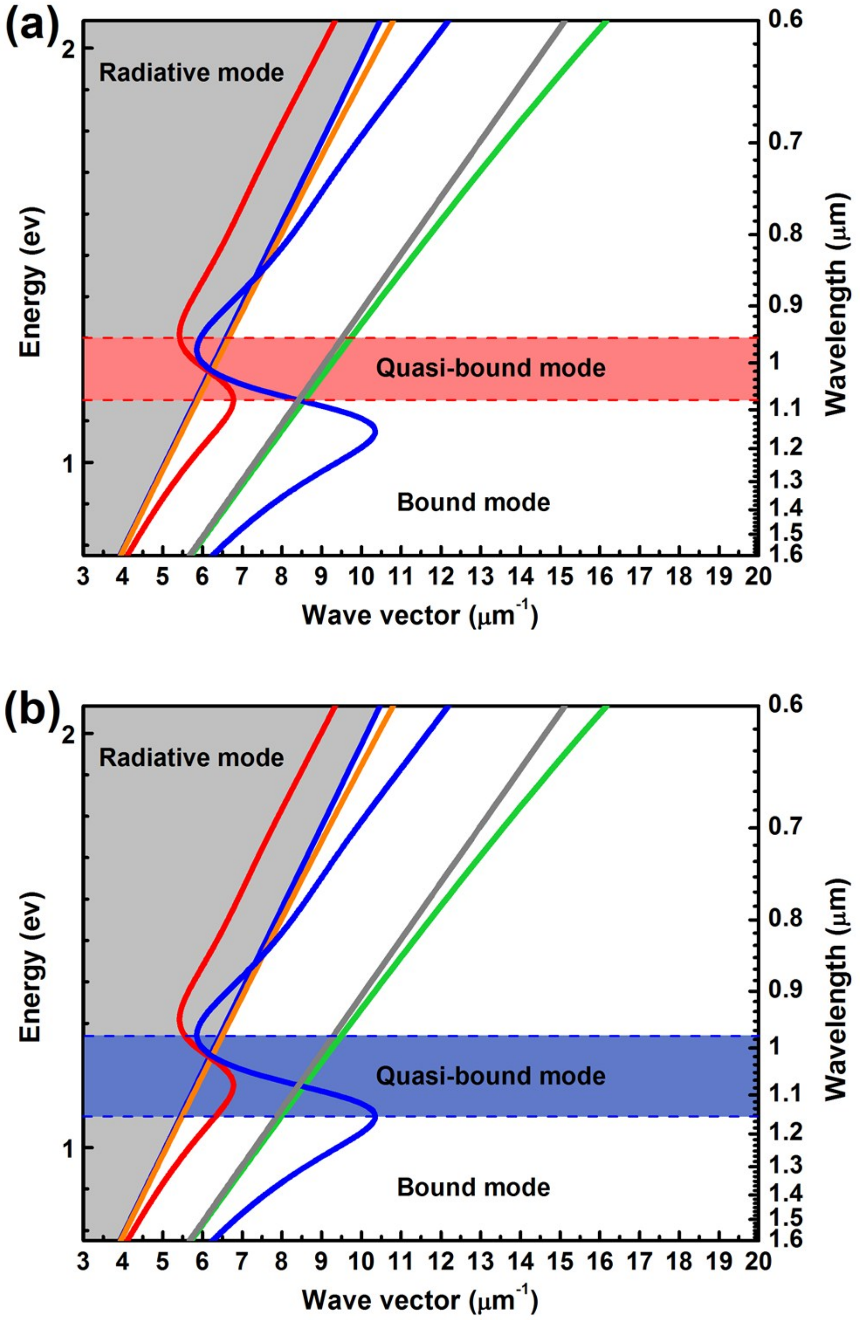

Supplementary Figure 3. (a)-(b) Dispersion relations of the fundamental modes at CaVO$_3$/air (red curve) and CaVO$_3$/silica (blue curve) interfaces. (a) Bound mode, quasi-bound mode and radiative mode for the CaVO$_3$/air configuration. The quasi-bound mode region is highlighted with a red rectangle bounded by red dashed lines. (b) Bound mode, quasi-bound mode and radiative mode for the CaVO$_3$/silica geometry. A blue rectangle with blue dashed lines at the top and bottom boundaries has been added to illustrate the quasi-bound mode region.

For the $CaVO_3$/air and $CaVO_3$/silica configurations, typical bound modes can be observed for energies below 1.15ev and 1.08ev, respectively. Above 1.3ev and 1.27ev, the onset of radiative modes can be seen for the two waveguides. Quasi-bound modes appear to exist for energies between the bound and radiative modes, as highlighted by the red and blue rectangles in Supplementary Figure 3. It is worth noting that the SPP waves at the Ag/dielectric interface exhibit a similar dispersion relationship at the near-ultraviolet frequencies [1]. Here, in order to compare the SPP modes supported by the Ag/dielectric interface at the near-ultraviolet frequencies, where they feature the maximum wavevector and confinement, and those guided by vandate-based configurations at the near-infrared, we plot the dispersion relationship, propagation loss and field profiles of these configurations within a much wider wavelength range (*i.e.* 250 nm ~ 1600 nm). It is clearly revealed in Supplementary Figure 4 that the transition between different mode states for Ag-based SPPs actually occurs at 3 to 4 ev. In addition, the wave-vectors and attenuations of the SPP modes at the near-ultraviolet are even larger than their vanadate counterparts at the near-infrared, along with more pronounced local field enhancement at the interface, indicating stronger light confinement capability. However, due to the fact that such behavior of Ag-based SPPs only occurs at high optical frequencies, vanadate materials (*e.g.* $CaVO_3$ and $SrVO_3$) are still more suitable candidates for applications at the optical communication bands due to their extreme field confinement exhibited in the near-infrared.

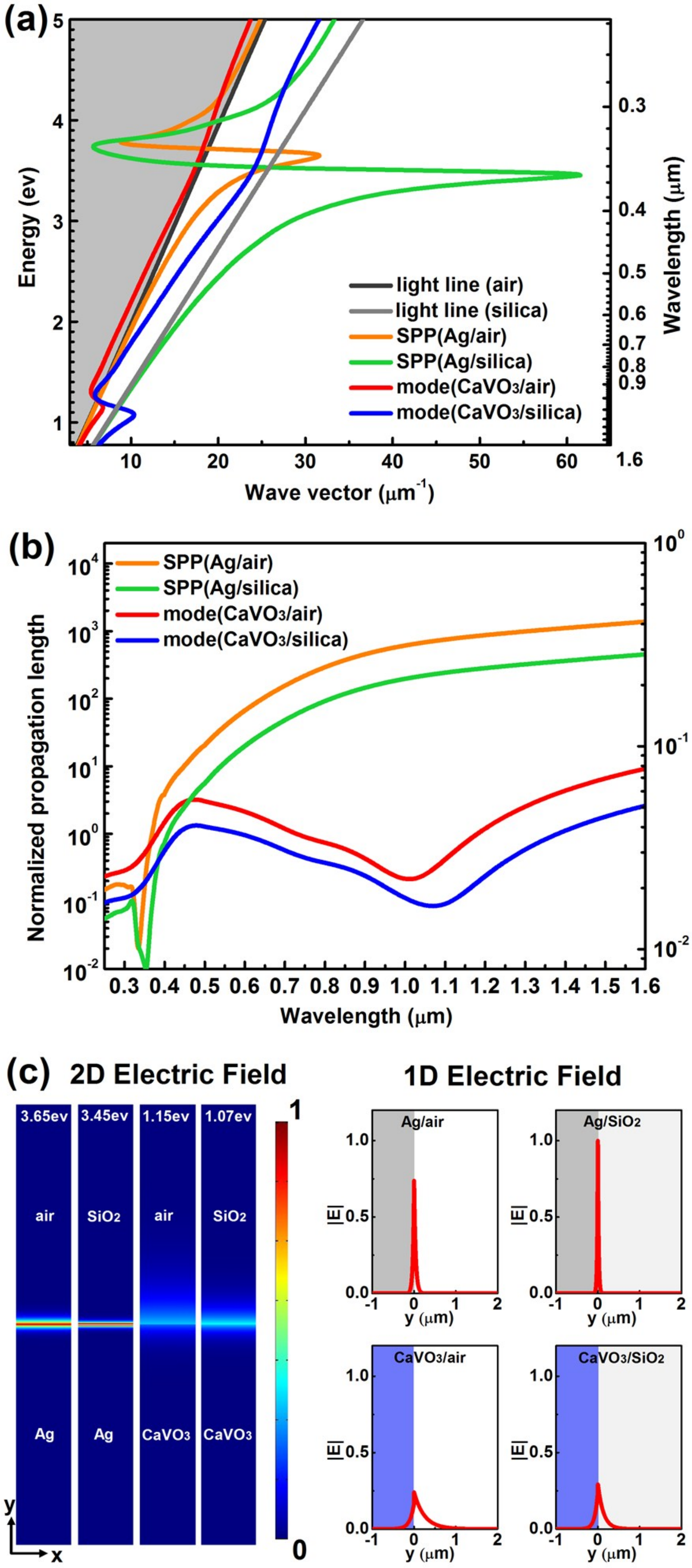

Supplementary Figure 4. (a) Dispersion relations of the fundamental guided modes at CaVO$_3$/air, CaVO$_3$/silica, Ag/air and Ag/silica interfaces within the wavelength range of 250 nm to 1600 nm.

(b) Normalized propagation lengths of the modes as a function of the operating wavelength. (c) 2D and 1D normalized electric field distributions of the guided fundamental modes for different configurations that demonstrate the largest wavevectors. Ag/air: E = 3.65 ev, λ = 340 nm; Ag/silica: E = 3.45 ev, λ = 359 nm; $CaVO_3$/air, E = 1.15ev, λ = 1078 nm; $CaVO_3$/silica, E = 1.07 ev, λ = 1158 nm.

In addition to the comparison of the $CaVO_3$- and Ag-based optical interfaces, here we also plot the dispersion curves for several other two-layer systems, including those based on $SrVO_3$, gold and ITO, as shown in Supplementary Figure 5. It is clearly seen that, within the considered energy range, the $SrVO_3$-based structures exhibit similar behavior as compared to the systems based on $CaVO_3$, although with different wave-vectors near the mode transition region. Similarly, SPPs at gold-based interfaces resemble those supported by a silver/dielectric system, with only slight differences in their wavevectors. Interestingly, modes at the ITO/dielectric interface demonstrate distinct behavior compared to the rest of these systems, with both ITO/air and ITO/silica dispersion curves lying inside the regions bounded by the dispersion relations of the light lines.

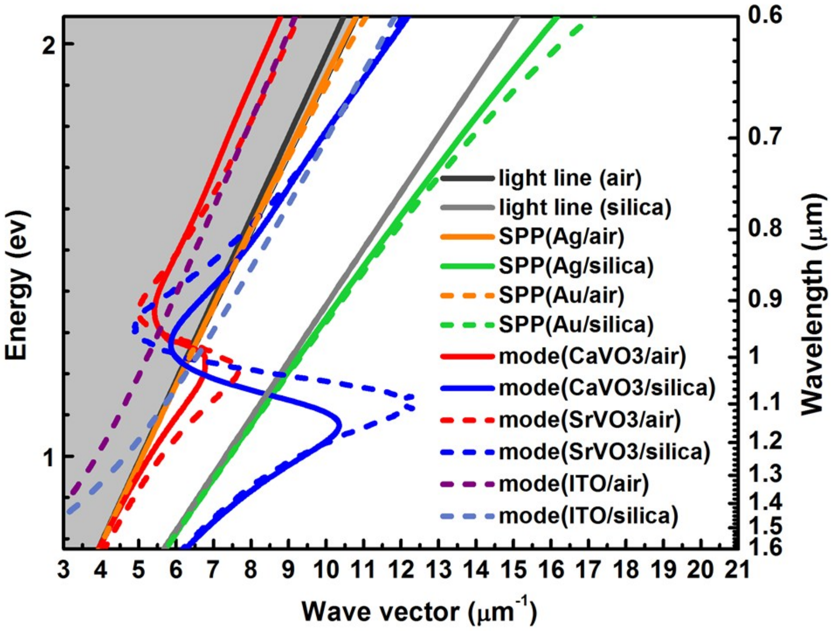

Supplementary Figure 5. Dispersion relations of the fundamental guided modes at $CaVO_3$/dielectric, $SrVO_3$/dielectric, Ag/dielectric, Au/dielectric and ITO/dielectric interfaces.

S3. Performance sensitivity of hybrid TE-pass polarizer to fabrication imperfections across 1.52 ~ 1.62 μm

In addition to the studies on the fabrication tolerance of the hybrid polarizer at 1.55 μm, we further investigate the wavelength dependence of the device performance against the considered fabrication errors. The results shown in Supplementary Figures 6-8 and Supplementary Tables 1-3 indicate that the optical performance of the TE-pass polarizer demonstrates a robust tolerance to such imperfections over a broadband wavelength range. Reasonable extinction ratios (17.3 ~ 37.7 dB) and low insertion losses (0.159 ~ 0.398 dB) can be realized simultaneously within a 1.52 ~ 1.62 μm range. These results further confirm the robustness of our proposed hybrid TE-pass polarizer.

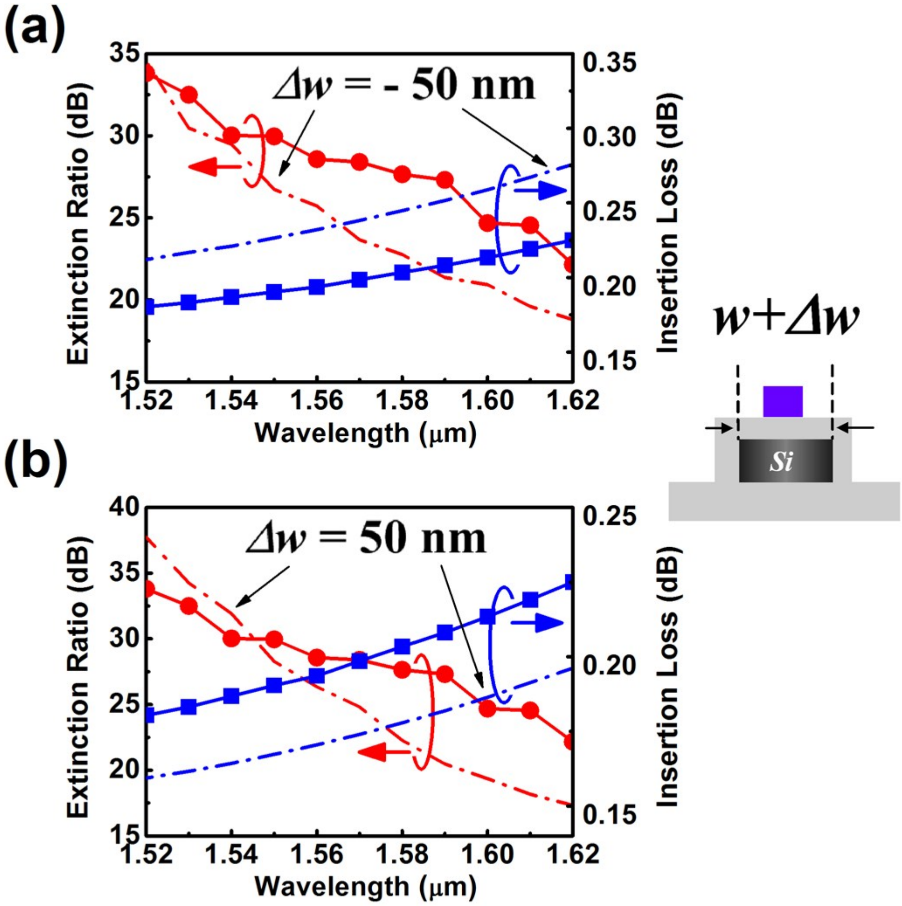

Supplementary Figure 6. Wavelength dependence of the hybrid polarizer with a ±50 nm width variation of the silicon ridge waveguide: (a) Δw = -50 nm; (b) Δw = 50 nm. Solid curves represent the performance results for the ideal device with no fabrication imperfections.

Supplementary Table 1. Summary of the device performance when the silicon ridge waveguide has a width variation of ±50 nm.

Structure (λ = 1.52 ~ 1.62 μm)	**Ideal Configuration**	**Δw = -50 nm**	**Δw = 50 nm**
ER (dB)	22.2 ~ 33.8	18.8 ~ 34.5	17.3 ~ 37.7
TE IL (dB)	0.18 ~ 0.225	0.212 ~ 0.276	0.159 ~ 0.196

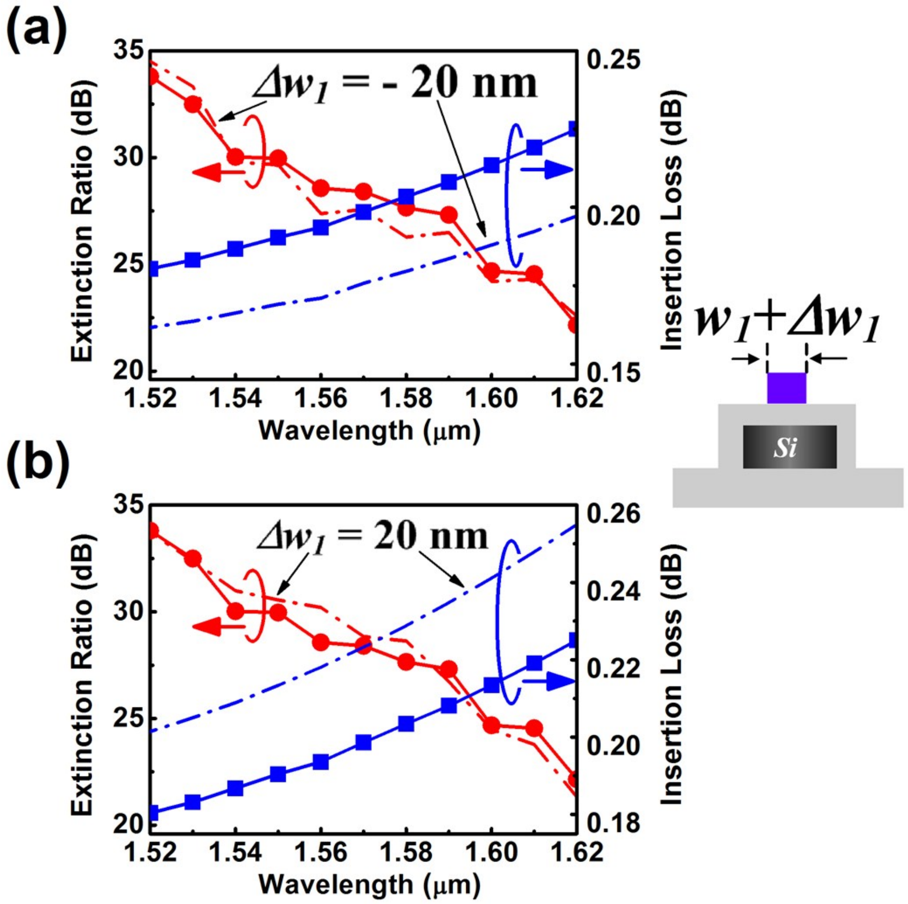

Supplementary Figure 7. Wavelength dependence of the hybrid polarizer with a ±20 nm width variation of the $CaVO_3$ nanowire: (a) Δw_1 = -20 nm; (b) Δw_1 = 20 nm. Solid curves correspond to the performance results of the ideal device with no fabrication imperfections.

Supplementary Table 2. Summary of the device performance when the $CaVO_3$ nanowire has a width variation of ±20 nm.

Structure (λ = 1.52 ~ 1.62 μm)	**Ideal Configuration**	**Δw_1= -20 nm**	**Δw_1 = 20 nm**
ER (dB)	22.2 ~ 33.8	22.6 ~ 34.5	21.3 ~ 33.7
TE IL (dB)	0.18 ~ 0.225	0.162 ~ 0.197	0.201 ~ 0.255

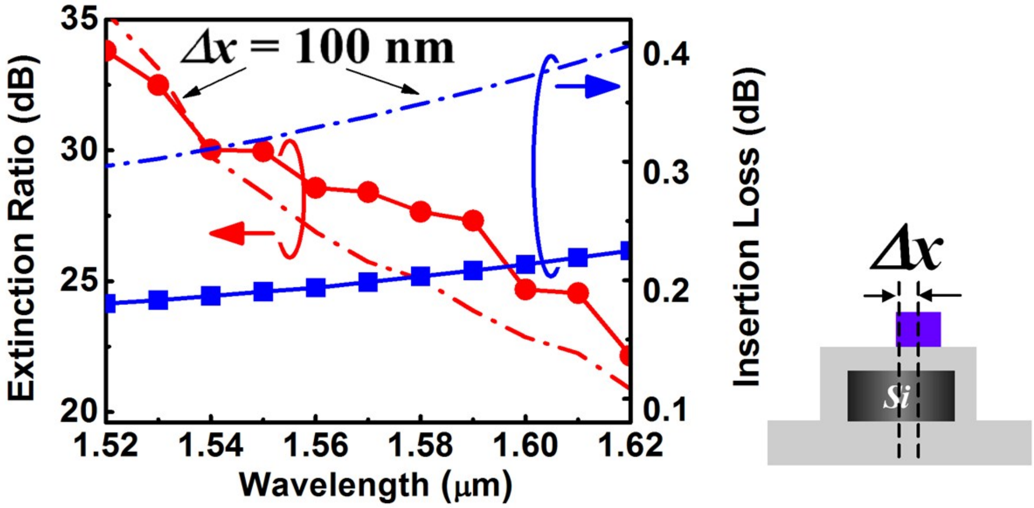

Supplementary Figure 8. Wavelength dependence of the hybrid polarizer with a deviated $CaVO_3$ nanowire (Δx = 100 nm). The extinction ratio and insertion loss of the ideal device with no fabrication error is plotted using solid curves to allow for a performance comparison.

Supplementary Table 3. Summary of the device performance when the $CaVO_3$ nanowire has a 100 nm deviation with respect to the silicon ridge waveguide.

Structure (λ = 1.52 ~ 1.62 μm)	**Ideal Configuration**	**Δx = 100 nm**
ER (dB)	22.2 ~ 33.8	20.9 ~ 35.3
TE IL (dB)	0.18 ~ 0.225	0.296 ~ 0.398

S4. Performance comparison with other polarizers based on transition metals, transition metal nitrides and ITO

In addition to the benchmarking against a Cr-based polarizer, here we conduct further comparisons with TE polarizers incorporating nanowires made of other types of materials instead of $CaVO_3$. These materials include transition metals such as V, Ti, and transition metal nitrides such as VN and TiN. The refractive indices of these materials are taken from [2]. In addition, an ITO-based polarizer has also been added to the comparison, where the material permittivity is taken from [3]. In the calculations, the dimension of the waveguide/nanowire cross-section and the length of the polarizer are set the same as those of the $CaVO_3$ polarizer and the wavelength is chosen at 1550 nm. Our results indicate that devices built upon the considered transition metals and transition metal nitrides demonstrate not only larger insertion loss (> 0.5 dB), but also smaller extinction ratios (< 20 dB) as compared to the vanadate-based polarizers. Though for the ITO case, lower TE insertion loss can be enabled (*i.e.* ~ 0.1 dB), the extinction ratio of the polarizer is significantly smaller (*i.e.* < 4.5 dB) than the device built upon vanadate materials. These results further confirm the superior performance of our proposed TE polarizer.

References

1. J. A. Dionne, L. A. Sweatlock, H. A. Atwater, and A. Polman, "Planar Metal Plasmon Waveguides: Frequency-dependent Dispersion, Propagation, Localization, and Loss Beyond the Free Electron Model," Phys. Rev. B **72**(7), 075405 (2005).
2. P. B. Johnson, and R. W. Christy, "Optical Constants of the Noble Metals," Phys. Rev. B **6**, 4370-4379 (1972).
3. H. W. Lee, G. Papadakis, S. P. Burgos, K. Chander, A. Kriesch, R. Pala, U. Peschel, and H. A. Atwater, "Nanoscale Conducting Oxide PlasMOStor," Nano Lett. **14**(11), 6463-6468 (2014).